crystals

MDPI

Article

Tribological Performance of Microcrystalline Diamond (MCD) and Nanocrystalline Diamond (NCD) Coating in Dry and Seawater Environment

Hui Zhang [1,2], Hui Song [2,*], Ming Pang [3,*], Guoyong Yang [2], Fengqin Ji [3,4], Nan Jiang [2,*] and Kazuhito Nishimura [5]

1 College of Transportation Science and Engineering, Civil Aviation University of China, Tianjin 300300, China
2 Key Laboratory of Marine Materials and Related Technologies, Zhejiang Key Laboratory of Marine Materials and Protective Technologies, Ningbo Institute of Materials Technology and Engineering (NIMTE), Chinese Academy of Sciences, Ningbo 315201, China
3 College of Aeronautical Engineering, Civil Aviation University of China, Tianjin 300300, China
4 State Key Laboratory of Solid Lubrication, Lanzhou Institute of Chemical Physics, Chinese Academy of Sciences, Lanzhou 730000, China
5 Advanced Nano-Processing Engineering Lab, Mechanical Engineering, Kogakuin University, Tokyo 192-0015, Japan
* Correspondence: songhui@nimte.ac.cn (H.S.); pangming1980@126.com (M.P.); jiangnan@nimte.ac.cn (N.J.)

Abstract: In the present study, the tribological properties of diverse crystalline diamond coating with micro (MCD) and nanometer (NCD) sizes, fabricated by the microwave plasma chemical vapor deposition (MPCVD) method, are systematically investigated in dry and seawater environments, respectively. Owing to the SiO_2 lubricating film with extraordinary hydrophilicity performance by a tribochemical reaction, the average friction coefficient (COF) and wear rate of NCD coating under seawater decreased by 37.8% and 26.5%, respectively, comparing with in dry conditions. Furthermore, graphite would be generated with the increment of surface roughness. Graphite transformed from the diamond under high contact pressure. Thus, with the synergism between SiO_2 lubricating film with extraordinary hydrophilicity performance and graphite, the corresponding COF and wear rate of MCD would be further decreased by up to 64.1% and 39.5%. Meanwhile, various characterizations on morphology, spectra, and tribological performance of the deposited diamond coating were conducted to explore the in-depth mechanism of the enhanced tribological performance of our NCD and MCD coatings in the extreme under seawater working conditions. We envision this work would provide significant insights into the wear behavior of diamond coatings in seawater and broaden their applications in protective coatings for marine science.

Keywords: diamond coating; tribological performance; seawater environment; lubricating film

check for updates

Citation: Zhang, H.; Song, H.; Pang, M.; Yang, G.; Ji, F.; Jiang, N.; Nishimura, K. Tribological Performance of Microcrystalline Diamond (MCD) and Nanocrystalline Diamond (NCD) Coating in Dry and Seawater Environment. *Crystals* **2022**, *12*, 1345. https://doi.org/10.3390/cryst12101345

Academic Editor: Hao Yi

Received: 30 August 2022
Accepted: 19 September 2022
Published: 23 September 2022

Publisher's Note: MDPI stays neutral with regard to jurisdictional claims in published maps and institutional affiliations.

Copyright: © 2022 by the authors. Licensee MDPI, Basel, Switzerland. This article is an open access article distributed under the terms and conditions of the Creative Commons Attribution (CC BY) license (https://creativecommons.org/licenses/by/4.0/).

1. Introduction

Chemical vapor deposition (CVD) polycrystalline diamond coatings have excellent mechanical properties, high thermal conductivity, and superior chemical inertness [1–3], which are widely applied in various fields [4–8]. Specially, polycrystalline diamond coatings as surface protection coatings possess a low coefficient of friction (COF), outstanding wear resistance, and high chemical stability, which shows great promise for applications in multifactor complex environment [9–11]. Moreover, polycrystalline diamond coatings with different morphologies and structures can be prepared by choosing the different deposition conditions of the CVD process such as the ratio of the reactive gas, the temperature, and the pressure of the substrate [12–15]. For example, the MCD coating deposited by CVD has excellent wear resistance and can be used in many fields, but its high surface roughness may lead to a high friction coefficient during the process of wear; the NCD coating has the characteristics of continuous film surface smoothness and other characteristics, which have good anti-friction performance during the process of wear [16]. Currently, scientists

have also conducted many in-depth studies on friction and wear properties of MCD and NCD coatings in some typical environments. Lei et al. [17] found that the friction coefficient of MCD and NCD after dry sliding was stable in the range of 0.053–0.062, whereas COF decreased to the range of 0.023–0.025 under water lubrication; De Barros Bouchet M I et al. [18] found that the ultra-low friction of NCD in the presence of water vapor was associated with OH and H passivation of the sliding surface, hydrogen-passivated surfaces were generated by dissociative adsorption of hydrogen molecules and were more effective than OH-terminated surfaces in further reducing friction. Cui et al. [19] investigated the tribological properties of fabricated polished MCD (MCD-p) films using a ball-plate reciprocating friction test with Si_3N_4 ceramic balls as counterparts under water lubrication, the grown MCD films, NCD films, and Si_3N_4 plates were used as comparison samples. MCD, NCD, and MCD-p films showed similar stable COF states after running in, which were 0.036, 0.032, and 0.035, respectively, and the wear rate of Si_3N_4 on MCD-p specimens was 2–3 orders of magnitude lower than the wear rate of sliding on grown MCD or NCD specimens. Feng et al. [20] studied that the friction coefficient of a diamond sliding in an ultra-high vacuum (UHV) (-4×10^{-9} Torr) was between 0.6 and 1.0, which was about ten times that was measured in air. However, in molecular gases at low pressure (-1×10^{-5} Torr), only oxygen leads to a significant reduction in the friction coefficient. Perle M et al. [6] deposited MCD coatings by a hot filament chemical vapor deposition process (HFCVD) and studied the friction properties under various atmospheres (oxygen, argon, nitrogen, ambient air); the displayed value of the coefficient of friction was in the range of 0.1 to 0.4. Lin et al. [21] investigated the frictional behavior of MCD and ultrananocrystalline diamond (UNCD) films at high temperatures, the results demonstrated that the wear of diamond film at 25–500 °C was mainly caused by the strong adhesion between diamond and substrate, and the wear resistance of UNCD film was significantly reduced by oxygen corrosion above 600 °C, whereas the MCD film still maintained a certain wear resistance at 700 °C. Furthermore, we have conducted a summary of current research into the friction and corrosion of several surface protective coatings in seawater. Wang et al. [22–24] have investigated the friction and corrosion mechanisms of Cr/GLC multilayered coating, 316 L stainless steel, and Al/Ti co-doped diamond-like carbon films in seawater. Ou et al. [25] have reported the superhard yet tough Ti-C-N coatings that showed excellent seawater-lubricating performance with an extremely low friction coefficient of 0.03 and a mild wear track in 3.5 wt% NaCl aqueous solution. Nonetheless, the current research on the friction and wear of diamond as a protective coating mainly focuses on the friction and wear behavior and related friction mechanism in a dry friction environment, water environment, even high-temperature environment, vacuum, low-pressure environment, and various atmospheric environment, and the friction and corrosion of diamond coatings have not studied in seawater. In fact, diamond has great application advantages as an anti-corrosion and wear-resistant material due to its high chemical stability. With the rapid development of marine equipment and marine technology, there is a high demand for surface protection materials of parts with high bearing capacity and sea-related friction, which requires that the protective material not only has good load-bearing capacity, but also maintains good lubricating properties under the boundary and fluid lubrication in the presence of seawater in order to ensure a satisfactory service life under severe working conditions [24–27]. However, the research on the tribological behavior of a diamond coating in a seawater environment has not been involved, and there is no research on the wear mechanism of common MCD and NCD coatings in a seawater environment. Considering the practical service condition will face a complex friction situation, in this study, both the tribological performance and corresponding friction mechanism of a typical diamond film in dry and seawater conditions have been studied exhaustively.

Bearing this aspect in mind, in this study, MCD and NCD coatings were prepared by MPCVD, we compared the friction and wear behavior of MCD and NCD coatings in a dry friction environment and simulated a seawater environment by carrying the friction test on a reciprocating ball-disk friction tester. Subsequently, we have systematically analyzed the

surface morphology, chemical composition changes, and phase evolution caused by sliding action in the worn areas, and thus revealed the frictional wear mechanism of different diamond coatings in a seawater environment.

2. Materials and Methods

2.1. Preparation of Diamond Coatings

In this experiment, we employed microwave plasma chemical vapor deposition (MPCVD, HMPS-2050, Provided by Ningbo Institute of Materials Technology and Engineering, Chinese Academy of Sciences, China) to grow the diamond coating. Single-side polished N (100) Si wafers (Bought from Zhejiang Lijing Silicon Material Co., Ltd., Jiaxing, China) whose thickness was 2 mm and an area of 2 × 2 cm^2 were used as substrates. Before the deposition process, the substrate was sequentially placed in acetone (Purchased from Sinopharm Chemical Reagent Co., Ltd., Shanghai, China) and alcohol (Bought from TAICANG XINTAI ALCOHOL CO., LTD., Suzhou, China) and sonicated for 5 min each. Afterward, two-step pretreatment was introduced on the substrates during the deposition to improve the nucleation density of diamond coatings. Firstly, the substrate specimens were sanded with sandpaper (2000 grit, Bought from SUISUN CO., LTD., Qingdao, China). Secondly, as shown in Figure 1a, the substrate specimens were seeded by ultrasonic oscillation with 200 nm diamond powder (Purchased from Zhongyuan Super Abrasives Co., Ltd., Zhengzhou, China) mixed with anhydrous ethanol solution in the ultrasonic device (KQ-100DE, KUNSHAN ULTRASONIC INSTRUMENT CO., LTD., Kunshan, China) for 10 min. After the seed crystal was completed, the surface was cleaned again by ultrasonic cleaned with anhydrous ethanol for 2 min. Thereafter, the treated substrate was dried with nitrogen gas and set aside in a dry place. Subsequently, as can be seen from Figure 1b, a microwave plasma chemical vapor deposition (MPCVD) with a rated power of 5 KW apparatus was applied for the MCD and NCD coatings deposition. The preparation parameters of MCD and NCD coatings are shown in Table 1. The MCD and NCD coatings were deposited with a ratio of CH_4/H_2 = 12/400 and a ratio of CH_4/H_2 = 20/400, respectively. A high gas pressure of 12 KPa was used during the MCD coatings deposition, and a low gas pressure of 9 KPa was used for the NCD coating process. In addition, an infrared thermometer (CHINO, IR-AH, Chino, Japan) was used to observe the deposition process of microwave chemical vapor deposition and measure the substrate temperature during the experiment. The substrate temperature of the MCD coatings was maintained at 900 ± 20 °C during the deposition growth, whereas the substrate temperature of the NCD coatings was kept at 670 ± 20 °C. The deposition time of MCD coating was 4 h and the deposition time of NCD coating was 9 h.

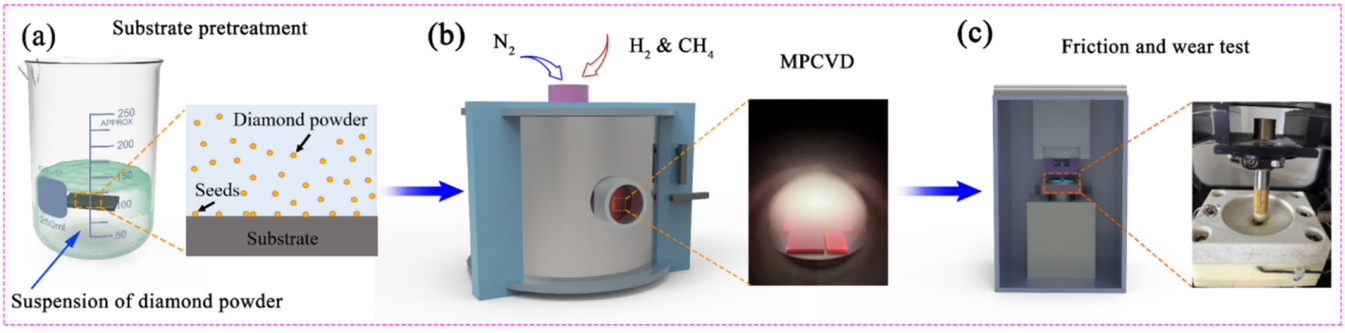

Figure 1. (**a**) Pretreatment of the substrate; (**b**) Preparation of diamond coating; (**c**) Testing of tribological properties.

Table 1. Synthesis parameters of MCD and NCD coatings.

	CH_4/sccm	H_2/sccm	N_2/sccm	Pressure/KPa	Power/KW	Substrate Temperature/°C
MCD	12	400	–	12	4.4	900 ± 20
NCD	20	400	20	9	3	670 ± 20

2.2. Friction and Wear Test

The tribological performance of the diamond coatings was carried out on ball-to-disk friction and wear tester (Rtec, Rtec Instruments, San Jose, CA, USA) configuration in reciprocating sliding mode. The test condition was at room temperature under a relative humidity of 50~80%. Then, the tribotests of MCD and NCD coatings were performed in the simulated sea environment (3.5 wt.% NaCl solution) and dry environment, respectively. SiC balls (Φ6 mm) were used as friction pairs after ultrasonic cleaned with ethanol and dried in air. The applied load was fixed at 15 N and the average sliding velocity of 20 mm/s with a stroke length of 4 mm for all tests, the test period was 5 h, and the friction coefficient of diamond coatings was recorded automatically by the friction tester. In order to reduce errors, every test was conducted at least three times. The schematic diagram of the tribological test is shown in Figure 1c

2.3. Characterization of Diamond Coatings

In order to obtain the precise surface morphology and structural information of as-prepared coatings, a scanning electron microscopy (SEM, Regulus8230, HITAGHI, Tokyo, Japan) at an accelerated voltage of 10 kV was used as characterization method to analyze the structural information of diamond coatings. The Raman spectrum of diamond coatings was measured by Raman spectrum (Raman, LabRAM Odyssey, HORIBA FRANCE SAS, Kyoto, Japan) with a wavelength of 532 nm. Atomic mechanics microscopy (AFM, Dimension 3100, Veeco, San Jose, CA, USA) was used to calculate the average roughness of MCD and NCD coatings. The cross-sectional transmission electron microscopy (TEM) sample was prepared on worn scars deposited at 960 °C using focused ion beam microscopy (FIB, Helios 5 CX, Thermo Fisher Scientific, Waltham, MA, USA). The TEM sample was cut along the direction perpendicular to the worn scars sliding. The microstructure of diamond and EDS analysis of lubricating film of the cross-sections of worn scars after the friction test were obtained by high-resolution transmission electron microscopy (HRTEM, Talos F200X, Thermo Fisher Scientific, Waltham, MA, USA) at 200 kV detailly. X-ray diffraction (XRD, D8 Advance, BRUKER, Madison, WI, USA) with a scanning rate of 8°/min was employed to determine the crystal structures of diamond coatings in the 10°–90° range (2θ). The contact angle of a seawater droplet on the diamond surface was measured by a contact angle measurement apparatus (DCAT21, Ningbo Jinmao Import and Export Co., Ltd., Ningbo, China) at a relative humidity of 50~80%. The chemical composition of MCD and NCD coatings before and after the friction test was determined using X-ray photoelectron spectroscopy (XPS, AXIS SUPRA, Kratos, Manchester, UK). A Revetest Scratch Test System (CSM Revetest, Ningbo Jinmao Import & Export Co., Ningbo, China) was conducted to test the adhesion of diamond coatings. A diamond tip with an applied normal load was increased from 0 N to 80 N, a scratching speed of 1 mm/min, and a scratching length was 5 mm. In order to reduce errors, all experiments were repeated at least three times.

3. Results

3.1. Characterization of As-Deposited Diamond Coatings

The surface and cross-sectional morphologies of as-deposited MCD and NCD coatings are observed by SEM, which are shown in Figure 2. Figure 2a shows the MCD coating has well-faceted crystallites exhibiting a rough surface, and the crystalline grain size of the MCD coating is about 10 μm. Unlike MCD coating, Figure 2d shows the NCD coating that was composed of small diamond particles which exhibited a smoother surface. As shown

in Figure 2e, grains on the NCD coating surface clustered and formed a typical cauliflower appearance, which could be clearly observed by SEM. Additionally, it can be clearly seen that continuous diamond coatings were deposited on the substrates, and the thicknesses of MCD and NCD coatings were 7.78 μm and 7.65 μm, respectively. The similar thicknesses of diamond coatings can eliminate the influence of the thickness on the properties of tribological performance. The size of NCD coatings cannot be distinguished individually from the SEM image due to the small grain size. We further analyzed the XRD pattern of the diamond coating surface as shown in Figure 2g. The average grain size of NCD can be determined using the (111) diffraction peak in the XRD pattern [28]. The diamond (111) peak of the NCD coating in Figure 2g was located at $2\theta = 44.68°$, according to Scherrer formula, and the average grain size of NCD coating was calculated at half of the maximum value of the diamond (111) peak [29,30]; therefore, the average grain size was calculated to be 20.8 nm. Figure 2h,i showed the Raman spectra of MCD and NCD coating, respectively. In the Raman spectrogram of the diamond coating, it can be clearly seen that there was a distinct peak at 1332 cm^{-1} all over, which proved the presence of sp^3 diamond phase. Furthermore, in the Raman spectrum of NCD coating, in addition to the characteristic peak of diamond out of 1332 cm^{-1}, there were also peaks of Raman shift at 1192.23 cm^{-1}, 1469.35 cm^{-1}, and 1556.27 cm^{-1}, respectively. The peaks 1192.23 cm^{-1} and 1469.35 cm^{-1} indicated the presence of the trans-polyacetylene (t-PA) phase, which was characteristic of nanoscale diamond particles [3,31–33], corresponding to the peak at 1556.27 cm^{-1} that was ascribed to graphite. This was attributed to the higher CH_4/H_2 concentration ratio and lower reaction gas pressure in the NCD coating deposition, and this raised the level of sp^2 impurities in the membrane [30]. However, in Raman spectroscopy, the sensitivity of graphite to Raman signals was tens of times higher than that of diamond [17]; therefore, it can be concluded that the diamond phase dominated in both coatings.

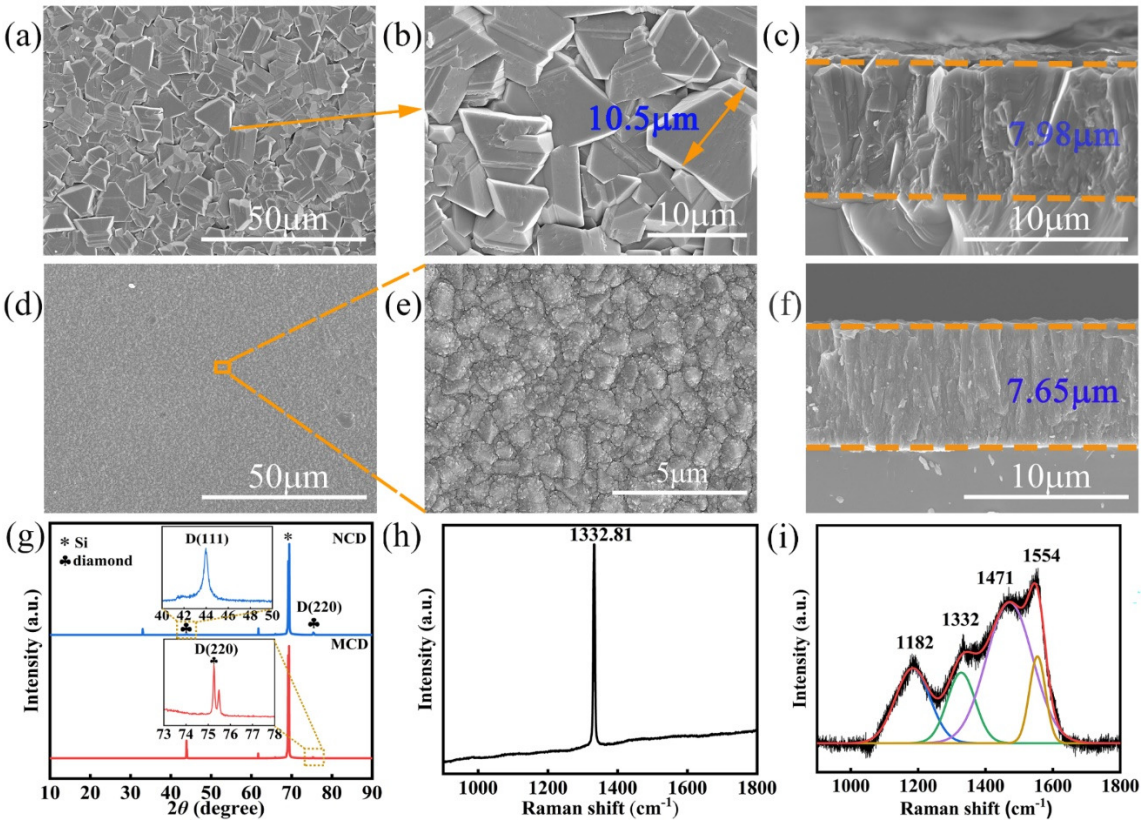

Figure 2. The surface and cross-sectional morphologies of diamond coatings: (**a**–**c**) MCD; (**d**–**f**) NCD; (**g**) The XRD pattern of diamond coatings; (**h**) The Raman spectrum of MCD coatings; (**i**) The Raman spectrum of NCD coatings.

The AFM topographies of different diamond films were acquired by AFM with a scanning range of 10 μm × 10 μm. The average roughness (Ra) of the coating was calculated by the software NanoScope Analysis. As illustrated in Figure 3a, the surface Ra of the MCD coating with obvious crystal spikes was calculated to be 248 nm. Compared with the MCD coating, the surface morphology of the NCD coating was relatively smooth, and the surface Ra of the NCD coating was calculated to be 51.9 nm. Figure 3b shows the wetting angle of seawater on MCD and NCD coatings. A surface is hydrophobic when its static wetting angle θ is >90° and hydrophilic when θ is <90° [34]. The wetting angle of seawater on NCD coating was 82.26°, whereas the MCD coating was 94.48°. Therefore, the NCD coating exhibited hydrophilic properties and the MCD coating exhibited hydrophobic properties. Figure 3c showed the scratch morphology of the MCD and NCD coatings as observed by the scratch test system. The first critical load when the film was peeled from the substrate can be used to assess the adhesion properties of the film [35]. The location of the MCD coating and the NCD coating peeled off from the substrate corresponded to loads of 73.1 N and 47.2 N, respectively. The more detailly Scratch morphologies of diamond are shown in Figure S1. This indicated that the adhesion of the MCD coating was better than NCD coating, which was consistent with the other works reported [36]. Furthermore, compared with other reports [36,37], our prepared MCD and NCD coatings have good adhesion properties.

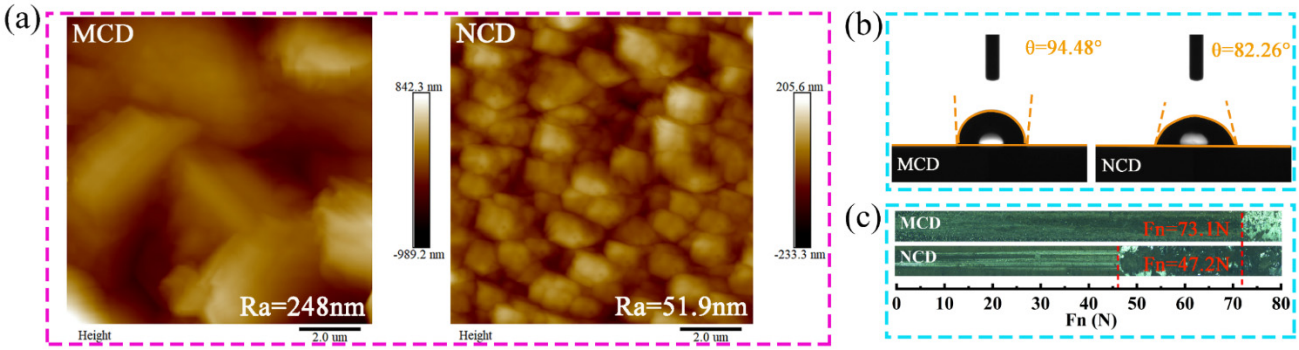

Figure 3. (**a**) The AFM three-dimensional morphologies of diamond coatings; (**b**) The wetting angle of the sea water on the diamond coatings; (**c**) Scratch morphologies of diamond coatings.

3.2. Tribological Performance of MCD and NCD Coatings

The COF of MCD and NCD coatings under different test conditions are given in Figure 4a,b, respectively. The results showed that the friction coefficient of diamond coating in the seawater environment was lower than in the dry friction environment. In Figure 4a,b, the friction coefficient has occurred obvious changes under the seawater environment. We compared the change in the average coefficient of friction for the first ten minutes and the last ten minutes of the wear process. For the MCD coating, in the dry environment, the coefficient of friction has changed from 0.3303 to 0.1509, and the friction coefficient of NCD coating has changed from 0.3343 to 0.0875. Furthermore, the coefficient of friction has changed from 0.1389 to 0.0360, and the friction coefficient of NCD coating has changed from 0.3304 to 0.0358 in seawater. This was contributed to by the seawater which can provide a certain thickness of the liquid film for the friction pairs in seawater lubrication conditions [17]; therefore, the roughness of the diamond coating surface was greatly reduced during the wear process and the actual contact area of the friction pair was minimized, thus reducing the coefficient of friction. In addition, the rough structure of the hydrophobic surface of the MCD coating may have also improved the load-bearing capacity of the friction pair, and reduced the friction coefficient. During hydrodynamic lubrication, the hydrodynamic effect was generated to achieve the synergistic effect of lubrication and anti-wear [38]. As shown in Figure 4a,b, the friction coefficient of MCD and NCD coatings showed a similar pattern of variation: the coefficient of friction rose rapidly during the initial period, which was due to the abrasive wear of ceramic balls rubbing on

the diamond coating and the plowing of microconvex bodies on the surface. Subsequently, all friction coefficients dropped rapidly to a steady state after a short break-in period [39]. Furthermore, compared with NCD coatings, MCD coatings reached the stabilization phase of COF in the seawater environment more quickly. In general, the diamond coatings have a lower COF in a seawater environment than in a dry friction environment, which may be related to the fluid lubrication effect in the liquid environment. In particular, as shown in Figure 4c, the average friction coefficient of MCD under dry friction environment was 0.1310, whereas the average friction coefficient of NCD coating was 0.1001. The MCD coatings have a higher COF in a dry friction environment due to the relatively rougher surface profile of MCD coatings resulting in a higher coefficient of friction. However, the friction coefficient in seawater environment showed an overall lower trend, the average friction coefficients of MCD and NCD coatings under seawater were 0.0402 and 0.0672, respectively. Compared with dry friction, the average friction coefficients of MCD and NCD coatings were reduced by 64.1% and 37.8%, respectively, and the wear rate was decreased by 39.5% and 26.5%, respectively. Figure 4c gives the wear rates of different diamond coatings under different test conditions. The formula for calculating the wear rate of a coating is as follows [32]:

$$W = \frac{V}{\mathrm{FL}} \quad (1)$$

Herein, W represents the wear rate and the unit is mm^3/Nm, V indicates the wear volume and the unit is μm^3, the unit of normal load (F) is N and the unit of wear scar length (L) is m. From Figure 4b, it can be seen that the wear rate of MCD coating was higher than that of NCD coating. Meanwhile, the wear rate of diamond coatings in the seawater environment was lower than those in the dry friction environment, which showed that the wear resistance of the diamond coating was better under the seawater environment.

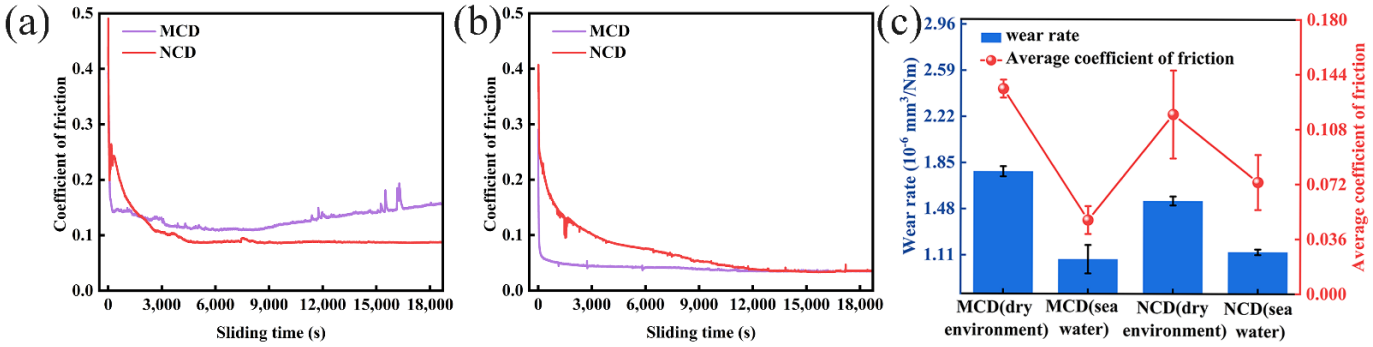

Figure 4. (**a**) Friction coefficient of diamond coatings in the dry environment; (**b**) Friction coefficient of diamond coatings in the seawater environment; (**c**) Average wear rate and average friction coefficient of diamond coatings.

3.3. Friction and Wear Analysis of Diamond Coatings in Dry Environment

In order to further investigate the corresponding wear mechanism, the worn morphology of different types of diamond film in every test condition was given in Figure 5. As shown in Figure 5a–h, in a dry friction environment, both MCD and NCD have more severe wear surfaces compared with a seawater environment, and it can be seen that the worn surface has obvious abrasive grains and scratches, and the rough surface generation and destruction may be closely related to their main friction mechanism under a dry friction environment. For MCD coating, obvious wear debris can be observed on the surface of the worn scars, as the surface of SiC balls was subjected to the sharp part of the diamond particles of the MCD coating with high shear stress during the process of wear. Moreover, the diamond particles also shattered during the process of wear, both SiC and diamond debris adhered to the diamond particles on the coating surface, and the counterpart ball surface also showed friction marks corresponding to the surface of the abrasion marks. The

surface was continuously smoothed so that the friction coefficient was relatively smooth after the running in period. However, most of the wear debris came from SiC balls which can be observed by EDS; the EDS analysis of the wear debris revealed debris consisting mainly of Si and O elements, the Si obtained from the SiC balls, and the O elements possibly associated with oxygen in the air (Figure S2, Supporting Information). The high hardness of the wear debris makes the surface of the SiC ball scratched and discontinuous, and the rough surface will fail rapidly due to scraping during repeated friction. For NCD coating, in Figure 5e,f, the worn scars of NCD coating was cleaner due to its smooth surface, as there was less wear debris left and the size was smaller. Its excellent dry friction performance could be contributed to its smoother surface, which should be closely related to the size of the grain scale. In general, the surface of the worn scars was significantly rougher and had deeper scratches under dry friction conditions; whereas, in the seawater environment, the width of the worn scars increased but the surface of the worn scars was smoother with only a slight scratch.

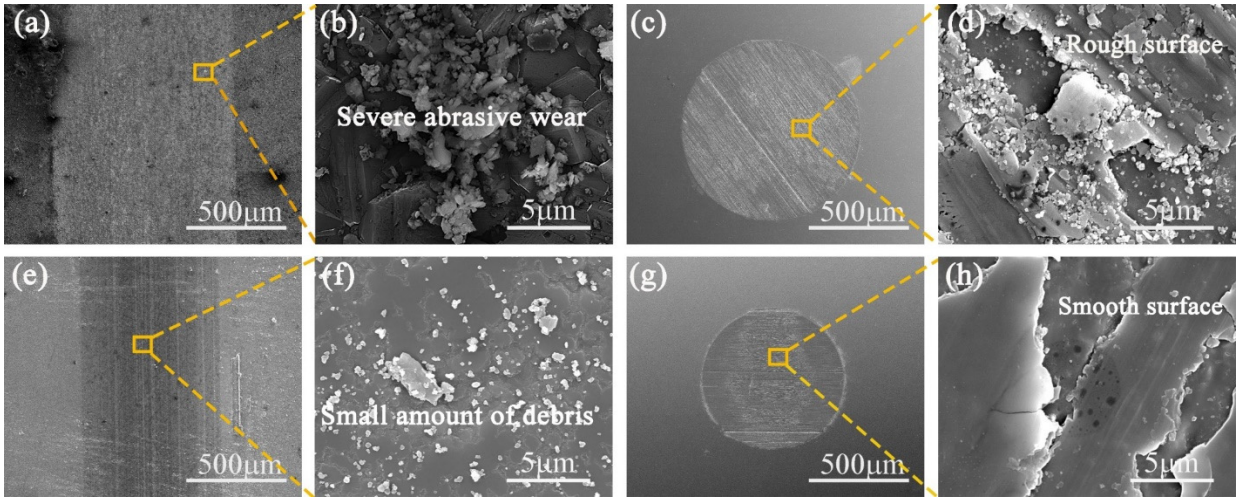

Figure 5. (**a**,**b**) The typical worn scars of MCD coatings sliding against SiC balls in the dry environment; (**c**,**d**) The typical worn scars of SiC sliding against MCD coatings in the dry environment; (**e**,**f**) The typical worn scars of NCD coatings sliding against SiC balls in the dry environment; (**g**,**h**) The typical worn scars of SiC sliding against NCD coatings in the dry environment.

Figure 6a,b show the Raman spectrum of diamond coating before and after friction in dry environment. It can be observed that the diamond peaks in the Raman spectrum show a right shift after the friction test, which was related to residual stress caused by the presence of non-diamond components and structural defects, such as rubbing process dislocations or impurities [17,39]. Moreover, the graphitic phase in the Raman spectrum after test increased compared with that before rubbing, which indicated that the diamond to graphite phase in the coating was transformed due to local pressure and shear stress during the process of wear [40]. Figure 6c–f are the XPS spectra of the worn scar surface before and after dry friction. It can be seen from the full spectra that the coating surface contained a higher oxygen concentration before friction, which was caused by the exposure of the coating to the atmospheric environment. After the dry friction test, the oxygen concentration on the coating surface increased, and the oxygen concentration of the NCD coating was higher than the MCD coating. In Figure 6d–f, C 1s spectra shows peaks at a bonding energy of 283.80 eV, 284.79 eV, and 286.42 eV before and after friction of the NCD coating, the peak at 283.80 eV corresponded to sp^2, and the peak at 284.79 eV represented sp^3. Furthermore, the peak at 286.42 eV represented CH_2-O/C=O which maybe originated from the friction pairs contacted with air during test. In contrast, the C 1s spectrum of the MCD coating before rubbing showed the two peaks at bonding energy of 284.78 eV and 286.50 eV, the peak at 284.78 eV corresponded to sp^3 and the peak at 286.50 eV represented

CH_2-O/C=O. After friction, there was an additional peak of MCD coating at 284.38 eV referred to sp^2 [39,41,42], which was because, during recurrent friction, the process of local pressure and shear stress and the heat generated by the relative motion may have caused sp^3 to sp^2 structural transformation which occurs at the friction contacts [43]. The graphite phase transition occurred by repeatedly applying compression (before ball contact) and tension (after ball contact) to the subsurface region of the wear track, and the formation of sp^2 bonds was easier to shear, resulting in a lower coefficient of friction [32,40]. In addition, it can be seen that the ratio of sp^2/sp^3 in the MCD and NCD coatings increased compared with those before friction, which indicated that the graphite phase increased after rubbing. This was consistent with the Raman spectroscopy results. Meanwhile, the sp^2 concentration of NCD coating was higher than MCD coating, which was known for low friction due to easy in-plane shearing [44,45]. This may be the reason for the better tribological properties of NCD under dry friction conditions.

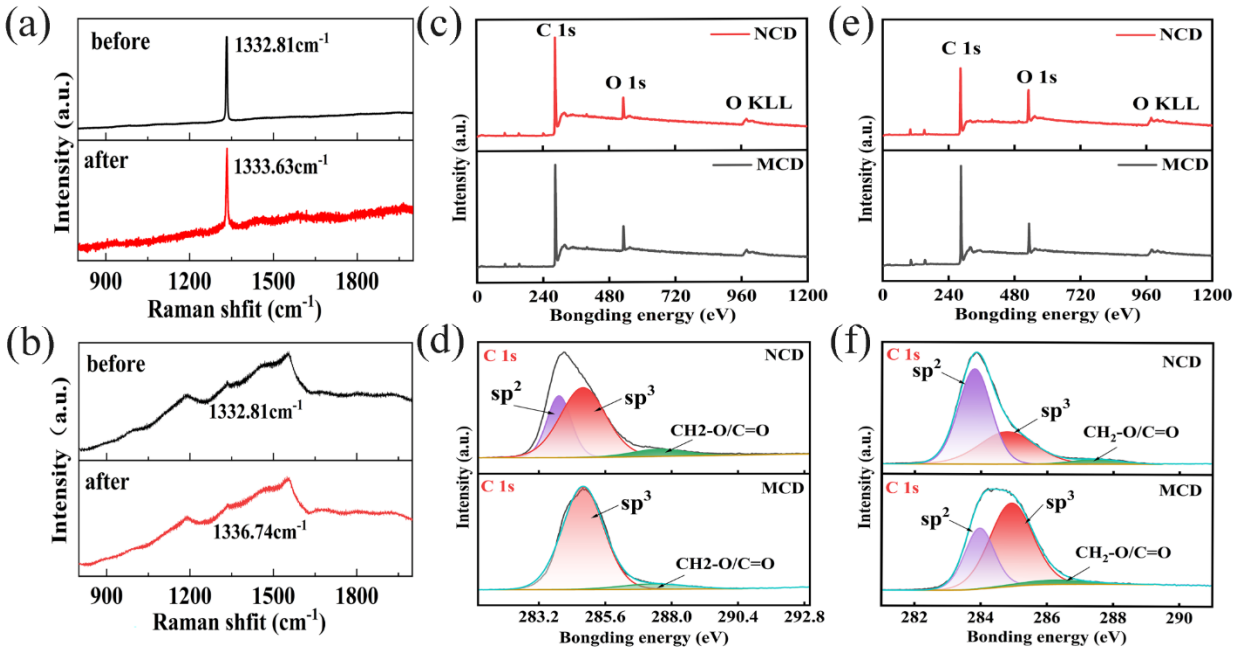

Figure 6. (**a**) The Raman spectrum of MCD coating before and afetr test; (**b**) The Raman spectrum of NCD coating before and afetr test; (**c**,**d**) The XPS spectra of the surface of the worn track before test; (**e**,**f**) The XPS spectra of the surface of the worn track after test under dry environment.

From the above analysis results, the wear mechanism of typical diamond coatings in the dry environment was mainly abrasive wear. The COF of the diamond coating was larger due to the three-body wear of the surface. Due to its rough surface, the MCD coating generated large wear debris during repeated wear and remained in the wear track, resulting in a high friction coefficient and serious wear. For NCD coating, the surface was smoother and produced less wear debris. From the XPS analysis results, the sp^2/sp^3 of the NCD coating surface was higher, indicating that the NCD surface produced more graphite, which reduced the friction coefficient. Therefore, the NCD coating has relatively excellent dry friction performance, which was consistent with the relevant literature reports [38,39,44,45].

3.4. The Influence of Seawater Environment on Friction Behavior of Diamond Coatings

To further investigate the wear mechanism of diamond coatings in a seawater environment, the wear morphology of MCD and NCD in a seawater environment is given in Figure 7a–h. As shown in Figure 7, the surface of the worn scars changed significantly compared to the dry friction environment, and the worn surface became smooth with only slight scratches. A friction-induced lubricating film has been observed on the worn surface of diamond film, which was distinguished from the morphology of coating in a dry

environment clearly. This indicated that the friction mechanism in a seawater environment was significantly different from that in a dry friction environment, and the formation of a lubricating film on the diamond surface may be related to the frictional chemical reaction in the seawater environment. As shown in Figure 7i,j, both MCD and NCD coatings produce a lubricating film on the surface. It can be observed that the thickness of the lubricating film of NCD can reach about 50 nm, whereas the lubricating film of MCD coating can reach about 200 nm. The MCD coating produced a thicker film. The EDS further confirm the composition of the cross-sectional morphologies of lubricating film. The main components of lubricating film were O and Si elements, where the O element may be adsorbed by atoms or molecules (e.g., H_2O, hydrogen and hydroxyl), the element Si was due to the SiC on the grinding ball in the friction process to produce grinding chips, a part of these abrasive chips in the friction will be expelled from the friction interface. The other part will be sandwiched between the two friction surfaces, and the lubricating film formed may be composed of SiO_2. In fact, under an applied load of 15 N, the degree of wear in these two environments was not significant for either MCD or NCD coatings, which may be related to the higher bonding force between the diamond and the substrate. In addition, the Na^+ and Cl^- in the seawater environment do not affect the surface of the diamond coating, indicating that the diamond coating has good anti-wear and anti-corrosion properties. Furthermore, more details about corrosion resistance were revealed, which were shown in Figure S3, and the corresponding analyses were exhibited in supporting information.

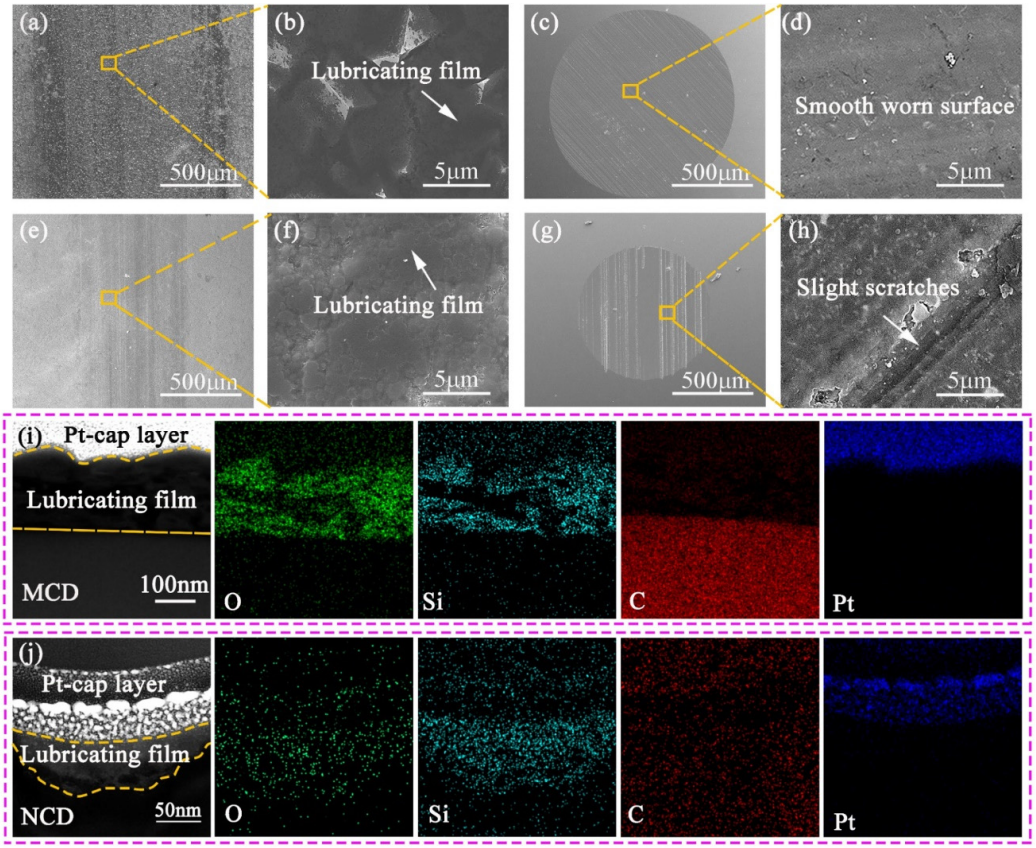

Figure 7. (**a**,**b**) The worn scars of MCD coatings sliding against SiC balls in the seawater environment; (**c**,**d**) The worn scars of SiC sliding against MCD coatings in the seawater environment; (**e**,**f**) The worn scars of NCD coatings sliding against SiC balls in the seawater environment; (**g**,**h**) The worn scars of SiC sliding against NCD coatings in the seawater environment; (**i**) The EDS mapping of the transfer film formed on the frictional zones of MCD diamond coatings; (**j**) The EDS mapping of the transfer film formed on the frictional zones of NCD diamond coatings.

Moreover, the worn scars of SiC balls sliding on NCD coating were all smaller than those on MCD coating under the same friction conditions, whereas SiC balls sliding on the MCD coating exhibited larger worn scars. These different worn profiles should be closely related to the different scales of diamond coating performance. The worn scars of SiC balls sliding on the MCD coating in the seawater environment were relatively large compared with the dry friction environment, which showed that the wear resistance of diamond coating was better under the seawater environment.

The X-ray photoelectron spectroscopy (XPS) spectra of C 1s, O 1s, and Si 2p on the worn surface under the sea water environment are given in Figure 8. The overall distribution of elements was shown in the Figure 8a. The two peaks of 99 eV and 150 eV corresponded to the Si 2p and Si 2s peaks, respectively. The spectra of C 1s was shown in Figure 8b. After friction and wear in the seawater environment, the surface of the worn scars of the MCD coating showed an increase in several components with a bonding energy of 283.89 eV, 285.34 eV, and 287.66 eV, respectively. The peak at 283.89 eV represented to sp^2; in addition, the peak of 285.34 eV represented the group of C-COO/CH_3/CH_2-O and the peak of 287.66 eV was corresponded to CH_2-O group, whereas the peak of sp^3 was located at the bonding energy of 284.78 eV. However, the surface of the worn scars of the NCD coating showed only three peaks at 283.45 eV, 284.80 eV, and 287.30 eV, respectively. The peak at 283.45 eV corresponded to sp^2, the peak at 284.80 eV represented sp^3, and the peak at 287.30 eV represented CH_2-O. It showed that there were various oxygen fragments and OH groups on the surface of the diamond coating after friction, which was due to the fact that the friction surface of the MCD coating was exposed to seawater in the seawater environment. Seawater contained a large amount of O and H elements. The spectra of Si 2p is shown in Figure 8c. On the worn scars of MCD and NCD coatings, the Si 2p spectra showed SiO_2 at a bonding energy of 103.36 eV [39,41,42], and the Si 2p spectra showed that more SiO_2 was generated on the surface of the MCD coating, which was consistent with the EDS results. The generated SiO_2 might have reduced the coefficient of friction during the friction process.

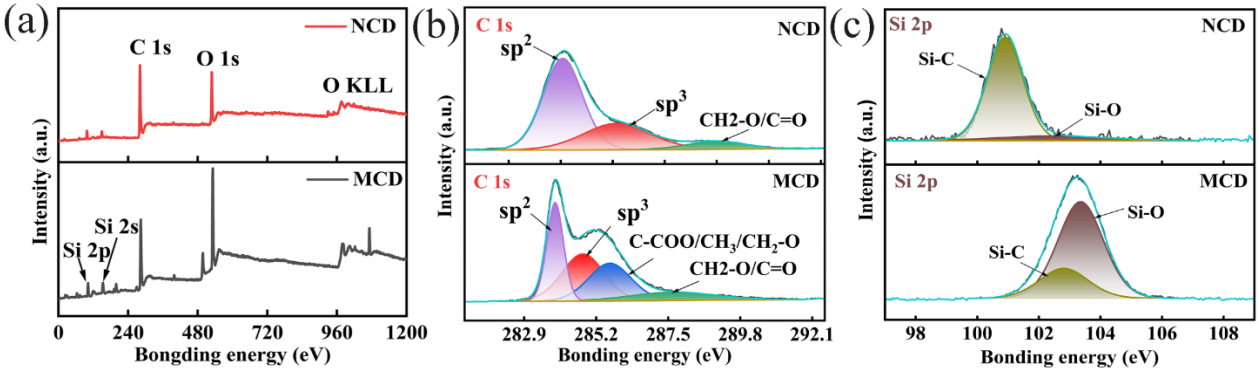

Figure 8. (**a**) The overall distribution of elements of the worn track in the seawater environment; (**b**) The C 1s spectra of the worn track in the seawater environment; (**c**) The Si 2p spectra of the worn track in the seawater environment.

In order to disclose the distinct tribological performance of above-mentioned coating, the subtle worn morphology was revealed in Figure 9, which shows the obtained TEM image of the wear scarred surface of the MCD and NCD coating and the corresponding SAED pattern. The TEM image in Figure 9a demonstrates the lubricating film on the surface of the MCD coating as well as the graphitization image close to the diamond surface. The diamond (111) lattice, graphite, and lubricating film were clearly separated by a dashed boundary marked in the HRTEM (high-resolution transmission electron microscope) image. The Fourier-transformed (FT) diffractogram image of Figure 9a is shown in the lower left inset, which indicated that both diamond (several of the diffraction points originated from diamond particles were marked by Dia) and nano-graphite (diffraction ring of graphite was

marked by G) were contained in the figure [46]. More details of the graphite and diamond area were unveiled with the zoom-in HRTEM image in Figures 9b and 9c, respectively. As presented in Figure 9b, the fringes of the lattice plane of graphite were clear, and it can be observed that the interplanar spacing of its G (200) orientation is 0.34 nm [47]; the FT diffractogram images of the graphite lattice structure inside the corresponding areas is exhibited in Figure 9(b1). Figure 9c showed that the fringes of the diamond lattice plane are clear, and the (111) lattice plane can be observed with a lattice spacing of 0.205 nm [48], which was the same structure as the crystalline diamond. The selected area electron diffraction image (SAED) of Figure 9c is shown in Figure 9(c1), which can be clearly observed in the diamond orientation of the (111) and (200) diffraction rings. The SAED of the diamond region provides a clearer pattern indicating the high quality and crystallinity of the diamond. The TEM image in Figure 9d shows the lubricating film on the surface of the NCD coating. As can be seen, compared with the MCD coating, only a lubricating film was formed on the surface of the NCD coating without the transformation of diamond to graphite phase. Under HRTEM investigation in Figure 9e, the (111) lattice plane can be observed with a lattice spacing of 0.206 nm. The FT diffractogram images of the diamond lattice structure inside the corresponding areas is shown in Figure 9(e1), which also can be clearly observed in the diamond orientation of the (111) and (200) diffraction rings.

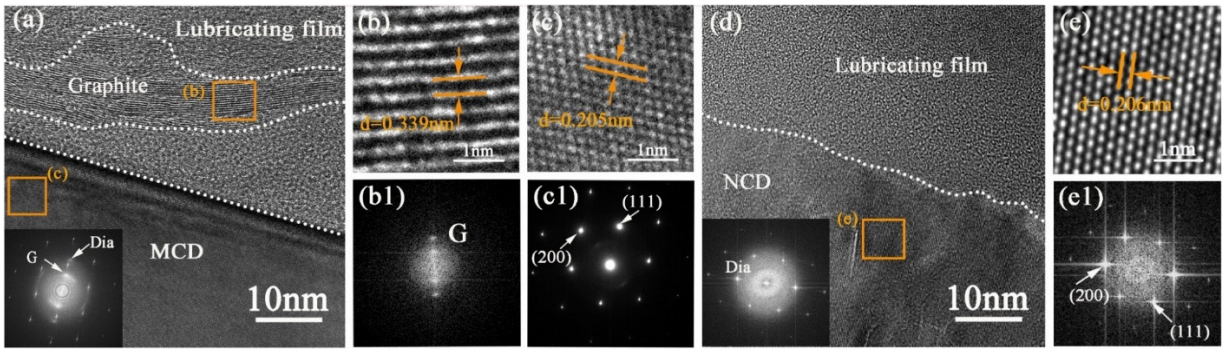

Figure 9. (**a**) The TEM image of the wear-scarred surface of the MCD coating; (**b**) HRTEM image of the graphite area of (**a**); (**b1**) the FT diffractogram images of (**b**); (**c**) HRTEM image of the diamond area of (**a**); (**c1**) the FT diffractogram images of (**c**); (**d**) The TEM image of the wear-scarred surface of the MCD coating; (**e**) HRTEM image of the diamond area of (**d**); (**e1**) the FT diffractogram images of (**e**).

From the above characterization results, the MCD coating and NCD coating have the effect of storing seawater due to their rough surfaces, so that a layer of water film was formed between the two worn surfaces, which hindered the direct contact between the two worn surfaces, resulting in a certain hydrodynamic effect for the low friction coefficient of the diamond coating in the seawater environment. In addition, the SiC wear debris generated during the friction process has a tribochemical reaction with water. The reaction process as follows [49–52]:

$$\text{Si-C} + H_2O \rightarrow \text{Si-OH} + \text{C-H}, \text{Si-OH} + \text{Si-OH} \rightarrow \text{O-Si-O} + H_2O$$

Therefore, the SiO_2 that was generated by a tribochemical reaction which formed a lubricating film on the surfaces of both the MCD coating and the NCD coating; SiO_2 lubricant films with high hydrophilicity retain water at the sliding interface. Retention of water at the sliding interface resulted in high load capacity and stable friction [52]. In addition, as the MCD coating has a rougher surface, a part of its surface area experienced a rather high local contact pressure, where the silica layer was destroyed by the contact force, and the asperity to the SiC ball surface and the diamond coating are sheared and destroyed, leaving the contact surface flat. Frictional heat is concentrated in the contact zone and the local temperature rises, leading to the transformation of sub-stable sp^3 bonds into stable

sp^2 bonds and graphitization of the contact area [53]. According to literature reports, in the case of graphite, its layered structure yields low friction only when the π–π* orbitals were separated by intercalated donors or acceptors. Water acts as a Lewis base (a weak donor for the high electron density of the π cloud), reducing the electron-hole attraction between the basal planes; therefore, the effect of water on graphite is to reduce its friction [17].

Based on the above analysis of the research results, we propose a feasible friction mechanism as shown in Figure 10. The surface of MCD coating in the dry friction environment was rough and the size of the generated wear debris was large, which led to severe abrasive wear during the repeated process of wear. In contrast, the surface of NCD coating was smoother, and the wear debris was smaller; in addition, more graphite was generated during the repeated process of wear, which made the NCD coating have better tribological properties in a dry environment. For the seawater environment, the excellent tribological properties of diamond coatings were attributed to the SiO_2 lubricant film generated by the tribochemical reaction, as is illustrated in Figure 10. Due to the micro-scale surface roughness of diamond, it was able to store water and wear debris between its grains, so that wear debris did not adhere between two wear surfaces and abrasive wear occurred. On the other hand, the SiO_2 generated by the tribochemical reaction also formed a lubricating film on the diamond surface, which was hydrophilic and therefore retained water at the sliding interface, both of which resulted in low friction and low wear of the diamond coating in a seawater environment. Furthermore, the MCD coating has a rougher surface, and the high local contact pressure allows the SiO_2 layer to break down. In these areas, the diamond phase produced a graphite phase change at high contact pressures and graphite also produced low frictional effects in water. Thus, for MCD coating in a seawater environment, the wear mechanism was a mixed lubrication state, with SiO_2 particles playing a major role. Although the graphite phase was formed at the top of the diamond surface asperity, the SiO_2 particles were also always generated at the wear interface and are always supplied to the lubricated interface, giving it a stable low friction state [54].

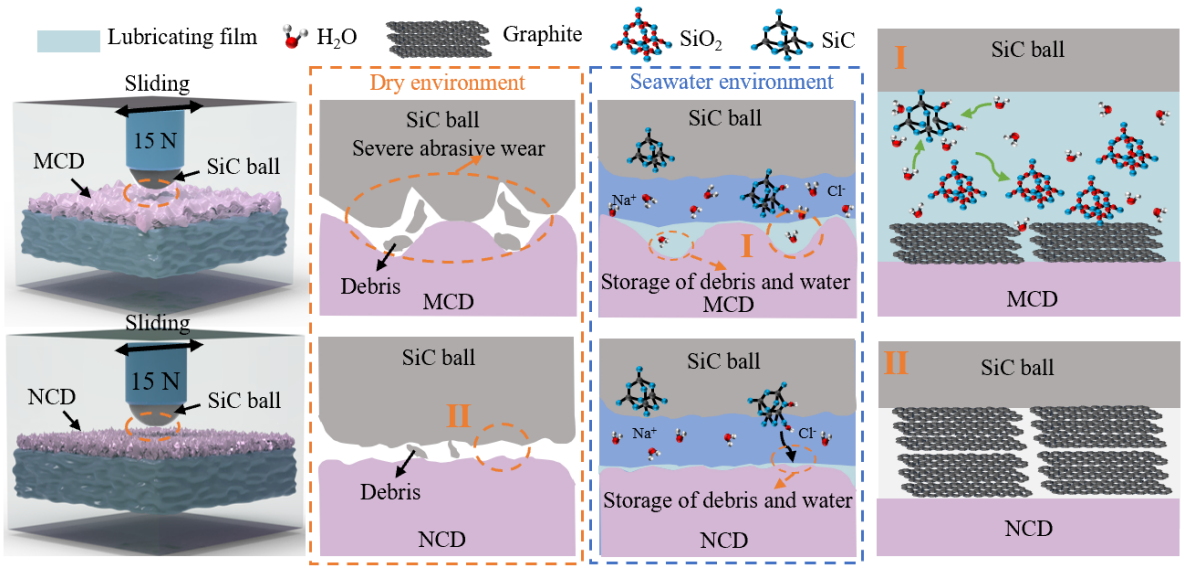

Figure 10. Schematic illustration of wear mechanism in dry friction and seawater environment.

4. Conclusions

In this study, MCD and NCD coatings were deposited by MPCVD, and the friction and wear behavior of the two coatings on diamond coatings in dry and seawater environments was investigated. This work provides significant insights into the sea water wear behavior of diamond coatings and the application of marine protective coatings. The main conclusions are as follows:

(1) Continuous and similar thicknesses of MCD and NCD coatings were successfully deposited by MPCVD under different deposition parameters, which eliminates the great influence of the thicknesses on the properties of tribological performance. Both MCD and NCD coatings have good bonding properties.
(2) The main wear mechanism of MCD coating and NCD coating in a dry friction environment is abrasive wear. The surface of the wear track of the NCD coating is smooth and the wear debris generated is small. Additionally, more sp^2 and graphite phases are generated in the wear track due to frictional heat, which makes the NCD coating have better tribological performance in a dry friction environment.
(3) Compared with the dry friction environment, the average COF of MCD and NCD coatings in the seawater environment are reduced 64.1% and 37.8%, respectively, and the wear rate is reduced by 39.5% and 26.5%, respectively. The main wear mechanism of the diamond coating is the SiO_2 lubricating film generated by the tribochemical reaction. Moreover, the MCD coating is a synergistic lubrication effect consisting of graphite phase and SiO_2 layer, resulting in a low average coefficient of friction and low wear.
(4) Based on the discussion on the friction mechanism of MCD and NCD coatings on diamond coatings in a dry environment and seawater environment, the diamond coating has good tribological properties and corrosion resistance in a seawater environment, which provides guidance on protective coatings on the surface of sea-related friction parts.

Supplementary Materials: The following supporting information can be downloaded at: https://www.mdpi.com/article/10.3390/cryst12101345/s1, Figure S1: (a) Scratch morphologies of MCD coatings in detail; (b) Scratch morphologies of NCD coatings in detail; Figure S2: (a) The EDS analysis of debris of MCD coating; (b) The EDS analysis of debris of NCD coating; Figure S3: (a) Nyquist plot for MCD coating obtained in a 3.5 wt.% NaCl solution; (b) Nyquist plot for NCD coating obtained in a 3.5 wt.% NaCl solution. (c) Bode plots for MCD and NCD coating were obtained in a 3.5 wt.% NaCl solution. References [55,56] are cited in the Supplementary Materials.

Author Contributions: Investigation, H.Z.; data curation, H.Z.; writing—original draft, H.Z.; writing—review and editing, H.S.; conceptualization, H.S. and M.P.; methodology, H.S. and M.P.; formal analysis, M.P.; supervision, N.J., F.J., G.Y., and K.N.; investigation, N.J., F.J., G.Y., and K.N. All authors have read and agreed to the published version of the manuscript.

Funding: The authors gratefully acknowledge the financial supports from the Open Project of the State Key Laboratory of Solid Lubrication (Grant No. LSL-2102), the Youth Fund of the Chinese Academy of Sciences (No. JCPYJJ-22030) and the Project of the Chinese Academy of Sciences (ZDKYYQ20200001).

Data Availability Statement: Not applicable.

Conflicts of Interest: The authors declare that they have no known competing financial interest or personal relationship that could have appeared to influence the work reported in this paper.

References

1. Gicquel, A.; Hassouni, K.; Silva, F.; Achard, J. CVD diamond films: From growth to applications. *Curr. Appl. Phys.* **2001**, *1*, 479–496. [CrossRef]
2. Wang, X.; Shen, X.; Sun, F.; Shen, B. Tribological properties of MCD films synthesized using different carbon sources when sliding against stainless steel. *Tribol. Lett.* **2016**, *61*, 1–16. [CrossRef]
3. Gaydaychuk, A.; Linnik, S. Tribological and mechanical properties of diamond films synthesized with high methane concentration. *Int. J. Refract. Met. Hard Mater.* **2019**, *85*, 105057. [CrossRef]
4. Wang, X.; Zhang, J.; Sun, F.; Zhang, T.; Shen, B. Investigations on the fabrication and erosion behavior of the composite diamond coated nozzles. *Wear* **2013**, *304*, 126–137. [CrossRef]
5. Chandran, M.; Kumaran, C.R.; Dumpala, R.; Shanmugam, P.; Natarajan, R.; Bhattacharya, S.S.; Ramachandra Rao, M.S. Nanocrystalline diamond coatings on the interior of WC–Co dies for drawing carbon steel tubes: Enhancement of tube properties. *Diamond Relat. Mater.* **2014**, *50*, 33–37. [CrossRef]

6. Perle, M.; Bareiss, C.; Rosiwal, S.M.; Singer, R.F. Generation and oxidation of wear debris in dry running tests of diamond coated SiC bearings. *Diamond Relat. Mater.* **2006**, *15*, 749–753. [CrossRef]
7. Sochr, J.; Švorc, Ľ.; Rievaj, M.; Bustin, D. Electrochemical determination of adrenaline in human urine using a boron-doped diamond film electrode. *Diamond Relat. Mater.* **2014**, *43*, 5–11. [CrossRef]
8. Chattopadhyay, A.; Sarangi, S.K.; Chattopadhyay, A.K. Effect of negative dc substrate bias on morphology and adhesion of diamond coating synthesised on carbide turning tools by modified HFCVD method. *Appl. Surf. Sci.* **2008**, *255*, 1661–1671. [CrossRef]
9. Miyake, S.; Shindo, T.; Miyake, M. Friction properties of surface-modified polished chemical-vapor-deposited diamond films under boundary lubrication with water and poly-alpha olefin. *Tribol. Int.* **2016**, *102*, 287–296. [CrossRef]
10. Ashcheulov, P.; Škoda, R.; Škarohlíd, J.; Taylor, A.; Fekete, L.; Fendrych, F.; Vega, R.; Shao, L.; Kalvoda, L.; Vratislav, S.; et al. Thin polycrystalline diamond films protecting zirconium alloys surfaces: From technology to layer analysis and application in nuclear facilities. *Appl. Surf. Sci.* **2015**, *359*, 621–628. [CrossRef]
11. Wang, X.; Shen, X.; Gao, J.; Wang, X.; Shen, X.; Gao, J.; Sun, F. Consecutive deposition of amorphous SiO2 interlayer and diamond film on graphite by chemical vapor deposition. *Carbon* **2017**, *117*, 126–136. [CrossRef]
12. Din, S.H.; Shah, M.A.; Sheikh, N.A.; Mursaleen Butt, M. CVD Diamond. *Trans. Indian Inst. Met.* **2019**, *72*, 1–9. [CrossRef]
13. Yang, Q.; Yang, S.; Li, Y.S.; Lu, X.; Hirose, A. NEXAFS characterization of nanocrystalline diamond thin films synthesized with high methane concentrations. *Diamond Relat. Mater.* **2007**, *16*, 730–734. [CrossRef]
14. Fabisiak, K.; Torz-Piotrowska, R.; Staryga, E.; Szybowicz, M.; Paprocki, K.; Banaszak, A.; Popielarski, P. The influence of working gas on CVD diamond quality. *Mater. Sci. Eng. C* **2012**, *177*, 1352–1357. [CrossRef]
15. Salgueiredo, E.; Amaral, M.; Neto, M.A.; Fernandes, A.J.S.; Oliveira, F.J.; Silva, R.F. HFCVD diamond deposition parameters optimized by a Taguchi Matrix. *Vacuum* **2011**, *85*, 701–704. [CrossRef]
16. Shabani, M.; Abreu, C.S.; Gomes, J.R.; Silva, R.F.; Oliveira, F.J. Effect of relative humidity and temperature on the tribology of multilayer micro/nanocrystalline CVD diamond coatings. *Diamond Relat. Mater.* **2017**, *73*, 190–198. [CrossRef]
17. Lei, X.; Shen, B.; Chen, S.; Wang, L.; Sun, F. Tribological behavior between micro-and nano-crystalline diamond films under dry sliding and water lubrication. *Tribol. Int.* **2014**, *69*, 118–127. [CrossRef]
18. De Barros Bouchet, M.I.; Zilibotti, G.; Matta, C.; Clelia Righi, M.; Vandenbulcke, L.; Vacher, B.; Martin, J.M. Friction of diamond in the presence of water vapor and hydrogen gas. Coupling gas-phase lubrication and first-principles studies. *J. Phys. Chem. C* **2012**, *116*, 6966–6972. [CrossRef]
19. Cui, Y.; He, Y.; Ji, C.; Lin, B.; Zhang, D. Anti-wear performance of polished microcrystalline diamond films sliding against Si3N4 under water lubrication. *Surf. Rev. Lett.* **2020**, *27*, 2050008. [CrossRef]
20. Feng, Z.; Tzeng, Y.; Field, J.E. Friction of diamond on diamond in ultra-high vacuum and low-pressure environments. *J. Phys. D Appl. Phys.* **1992**, *25*, 1418. [CrossRef]
21. Lin, Q.; Chen, S.; Ji, Z.; Huang, Z.; Zhang, Z.; Shen, B. High-temperature wear behavior of micro-and ultrananocrystalline diamond films against titanium alloy. *Surf. Coat. Technol.* **2021**, *422*, 127537. [CrossRef]
22. Liu, Y.; Li, S.; Li, H.; Ma, G.; Sun, L.; Guo, P.; Ke, P.; Lee, K.R.; Wang, A. Controllable defect engineering to enhance the corrosion resistance of Cr/GLC multilayered coating for deep-sea applications. *Corros. Sci.* **2022**, *199*, 110175. [CrossRef]
23. Liu, Y.; Liu, L.; Li, S.; Wang, R.; Guo, P.; Wang, A.; Ke, P. Accelerated deterioration mechanism of 316L stainless steel in NaCl solution under the intermittent tribocorrosion process. *J. Mater. Sci. Technol.* **2022**, *121*, 67–79. [CrossRef]
24. Xu, X.; Guo, P.; Zuo, X.; Sun, L.; Li, X.; Lee, K.R.; Wang, A. Understanding the effect of Al/Ti ratio on the tribocorrosion performance of Al/Ti co-doped diamond-like carbon films for marine applications. *Surf. Coat. Technol.* **2020**, *402*, 126347. [CrossRef]
25. Ou, Y.; Wang, H.; Hua, Q.; Liao, B.; Ouyang, X. Tribocorrosion behaviors of superhard yet tough Ti-CN ceramic coatings. *Surf. Coat. Technol.* **2022**, *439*, 128448. [CrossRef]
26. Dong, M.; Zhu, Y.; Xu, L.; Ren, X.; Ma, F.; Mao, F.; Li, J.; Wang, L. Tribocorrosion performance of nano-layered coating in artificial seawater. *Appl. Surf. Sci.* **2019**, *487*, 647–654. [CrossRef]
27. Wang, X.; Jiang, Y.; Wang, Y.; Ye, C.; Du, C. Probing the tribocorrosion behaviors of three nickel-based superalloys in sodium chloride solution. *Tribol. Int.* **2022**, *172*, 107581. [CrossRef]
28. Wang, H.; Wang, C.; Wang, X.; Sun, F. Effects of carbon concentration and gas pressure with hydrogen-rich gas chemistry on synthesis and characterizations of HFCVD diamond films on WC-Co substrates. *Surf. Coat. Technol.* **2021**, *409*, 126839. [CrossRef]
29. Patterson, A.L. The Scherrer formula for X-ray particle size determination. *Phys. Rev.* **1939**, *56*, 978. [CrossRef]
30. Wang, H.; Song, X.; Wang, X.; Sun, F. Fabrication, tribological properties and cutting performances of high-quality multilayer graded MCD/NCD/UNCD coated PCB end mills. *Diamond Relat. Mater.* **2021**, *118*, 108505. [CrossRef]
31. Klauser, F.; Steinmüller-Nethl, D.; Kaindl, R.; Bertel, E.; Memmel, N. Raman studies of nano-and ultra-nanocrystalline diamond films grown by hot-filament CVD. *Chem. Vap. Depos.* **2010**, *16*, 127–135. [CrossRef]
32. Sharma, N.; Kumar, N.; Dhara, S.; Dash, S.; Bahuguna, A.; Kamruddin, M.; Tyagi, A.K.; Raj, B. Tribological properties of ultra nanocrystalline diamond film-effect of sliding counterbodies. *Tribol. Int.* **2012**, *53*, 167–178. [CrossRef]
33. Kumar, N.; Kozakov, A.T.; Sankaran, K.J.; Sidashov, A.V.; Lin, I.N. Controlled atmosphere dependent tribological properties of thermally annealed ultrananocrystalline diamond films. *Diamond Relat. Mater.* **2019**, *97*, 107437. [CrossRef]

34. Law, K.Y. Definitions for hydrophilicity, hydrophobicity, and superhydrophobicity: Getting the basics right. *J. Phys. Chem. Lett.* **2014**, *5*, 686–688. [CrossRef]
35. Song, H.; Ji, L.; Li, H.; Liu, X.; Zhou, H.; Liu, L.; Chen, J. Interface design for aC: H film with super long wear life in high vacuum environment. *Tribol. Int.* **2016**, *95*, 298–305. [CrossRef]
36. Yan, G.; Wu, Y.; Cristea, D.; Liu, L.; Tierean, M.; Wang, Y.; Lu, F.; Wang, H.; Yuan, Z.; Munteanu, D.; et al. Mechanical properties and wear behavior of multi-layer diamond films deposited by hot-filament chemical vapor deposition. *Appl. Surf. Sci.* **2019**, *494*, 401–411. [CrossRef]
37. Buijnsters, J.G.; Shankar, P.; Van Enckevort, W.J.P.; Schermer, J.J.; Ter Meulen, J.J. Adhesion analysis of polycrystalline diamond films on molybdenum by means of scratch, indentation and sand abrasion testing. *Thin Solid Films* **2005**, *474*, 186–196. [CrossRef]
38. Guo, Y.; Zhu, Y.; Zhang, X.; Luo, B. Effects of Superhydrophobic Surface on Tribological Properties:Mechanism, Status and Prospects. *Prog. Chem.* **2020**, *32*, 320. [CrossRef]
39. Wang, C.; Wang, X.; Sun, F. Tribological behavior and cutting performance of monolayer, bilayer and multilayer diamond coated milling tools in machining of zirconia ceramics. *Surf. Coat. Technol.* **2018**, *353*, 49–57. [CrossRef]
40. Voevodin, A.A.; Phelps, A.W.; Zabinski, J.S.; Donley, M.S. Friction induced phase transfor-mation of pulsed laser deposited diamond-like carbon. *Diamond Relat. Mater.* **1996**, *5*, 1264–1269. [CrossRef]
41. Kumar, N.; Sankaran, K.J.; Kozakov, A.T.; Sidashov, A.V.; Nicolskii, A.V.; Haenen, K.; Kolesnikov, V.I. Surface and bulk phase analysis of the tribolayer of nanocrystalline diamond films sliding against steel balls. *Diamond Relat. Mater.* **2019**, *97*, 107472. [CrossRef]
42. Huang, K.; Hu, X.; Xu, H.; Shen, Y.; Khomich, A. The oxidization behavior and mechanical properties of ultrananocrystalline diamond films at high temperature annealing. *Appl. Surf. Sci.* **2014**, *317*, 11–18. [CrossRef]
43. Erdemir, A.; Fenske, G.R.; Krauss, A.R.; Gruen, D.M.; McCauley, T.; Csencsits, R.T. Tribological properties of nanocrystalline diamond films. *Surf. Coat. Technol.* **1999**, *120*, 565–572. [CrossRef]
44. Abreu, C.S.; Oliveira, F.J.; Belmonte, M.; Fernandes, A.J.S.; Gomes, J.R.; Silva, R.F. CVD diamond coated silicon nitride self-mated systems: Tribological behaviour under high loads. *Tribol. Lett.* **2006**, *21*, 141–151. [CrossRef]
45. Kumar, N.; Panda, K.; Dash, S.; Popov, C.; Reithmaier, J.P.; Panigrahi, B.K.; Tyagi, A.K. Baldev Raj. Tribological properties of nanocrystalline diamond films deposited by hot filament chemical vapor deposition. *AIP Adv.* **2012**, *2*, 032164. [CrossRef]
46. Chen, C.; Fan, D.; Xu, H.; Jiang, M.; Li, X.; Lu, S.; Ke, C.; Hu, X. Monoatomic tantalum induces ordinary-pressure phase transition from graphite to n-type diamond. *Carbon* **2022**, *196*, 466–473. [CrossRef]
47. Shen, B.; Ji, Z.; Lin, Q.; Gong, P.; Xuan, N.; Chen, S.; Liu, H.; Huang, Z.; Xiao, T.; Sun, Z. Graphenization of Diamond. *Chem. Mater.* **2022**, *34*, 3941–3947. [CrossRef]
48. Lu, Y.; Man, W.; Wang, B.; Rosenkranz, A.; Yang, M.; Yang, K.; Yi, J.; Song, H.; Li, H.; Jiang, N. (100) oriented diamond film prepared on amorphous carbon buffer layer containing nano-crystalline diamond grains. *Surf. Coat. Technol.* **2020**, *385*, 125368. [CrossRef]
49. Gates, R.S.; Hsu, S.M. Tribochemistry between water and Si3N4 and SiC: Induction time analysis. *Tribol. Lett.* **2004**, *17*, 399–407. [CrossRef]
50. Ootani, Y.; Xu, J.; Adachi, K.; Kubo, M. First-principles molecular dynamics study of silicon-based ceramics: Different tribochemical reaction mechanisms during the running-in period of silicon nitride and silicon carbide. *J. Phys. Chem. C* **2020**, *124*, 20079–20089. [CrossRef]
51. Wang, Y.; Yukinori, K.; Koike, R.; Ootani, Y.; Adachi, K.; Kubo, M. Selective Wear Behaviors of a Water-Lubricating SiC Surface under Rotating-Contact Conditions Revealed by Large-Scale Reactive Molecular Dynamics Simulations. *J. Phys. Chem. C* **2021**, *125*, 14957–14964. [CrossRef]
52. Kasuya, M.; Hino, M.; Yamada, H.; Mizukami, M.; Mori, H.; Kajita, S.; Ohmori, T.; Suzuki, A.; Kurihara, K. Characterization of Water Confined between Silica Surfaces Using the Resonance Shear Measurement. *J. Phys. Chem. C* **2013**, *117*, 13540–13546. [CrossRef]
53. Li, J.; Yu, X.; Zhang, Z.; Zhao, Z. Exploring a diamond film to improve wear resistance of the hydraulic drilling impactor. *Surf. Coat. Technol.* **2019**, *360*, 297–306. [CrossRef]
54. Ootani, Y.; Xu, J.; Nakamura, F.; Kawaura, M.; Uehara, S.; Kanda, K.; Wang, Y.; Ozawa, N.; Adachi, K.; Kubo, M. Three Tribolayers Self-Generated from SiC Individually Work for Reducing Friction in Different Contact Pressures. *J. Phys. Chem. C* **2022**, *126*, 2728–2736. [CrossRef]
55. Ponthiaux, P.; Wenger, F.; Drees, D.; Celis, J.P. Electrochemical techniques for studying tribocorrosion processes. *Wear* **2004**, *256*, 459–468. [CrossRef]
56. Namus, R.; Rainforth, W.M. The influence of cathodic potentials on the surface oxide layer status and tribocorrosion behaviour of Ti6Al4V and CoCrMo alloys in simulated body fluid. *Biotribology* **2022**, *30*, 100212. [CrossRef]